


Fusion power supply advances by the J-TEXT engineering team

Ming ZHANG (张明), Hongqi ZHANG (张鸿淇), Rumeng WANG (王如梦) , Xiaohan XIE (谢筱涵), Wenshan WANG (王文山), Yixing JIANG (江易星), Zhiheng LI (李志恒), Peilong ZHANG (张沛龙), Liye WANG (王俐晔), Shaoxiang MA (马少翔)*, Yong YANG (杨勇), Wei ZHENG (郑玮) and Bo RAO (饶波)

International Joint Research Laboratory of Magnetic Confinement Fusion and Plasma Physics, State Key Laboratory of Advanced Electromagnetic Engineering and Technology and School of Electrical and Electronic Engineering, Huazhong University of Science and Technology, Wuhan 430074, People's Republic of China

E-mail: mashaoxiang@hust.edu.cn

Received 9 September 2022, revised 25 October 2022

Accepted for publication 1 November 2022

Published 30 November 2022



CrossMark

Abstract

To meet the stringent requirements of the fusion power supply for large-scale fusion devices, the J-TEXT engineering team has carried out key technology research and applications in several important directions of fusion power supply. This article presents the advances made by the J-TEXT engineering team in recent years in the following areas: (1) a high-voltage power supply for an auxiliary heating system; (2) a breakdown protection device for an auxiliary heating power supply; (3) magnetic field compatibility; (4) a high-voltage pulsed power supply for a field-reversed configuration; (5) a large physics experimental facility control system. The research backgrounds, technical progress, test results, applications, summaries and prospects are described in detail in each part. These innovative research results and valuable engineering experience can promote the progress of fusion power supply technology, and also lay a foundation for the development of power supplies with higher parameters in the future.

Keywords: high-voltage DC power supply, breakdown protection, magnetic field compatibility, high-voltage pulsed power supply, control system

(Some figures may appear in colour only in the online journal)

1. Introduction

The requirements for a fusion power supply are becoming increasingly stringent as fusion research and device development progress [1]. Depending on the operating conditions, there are two types of fusion power supplies: steady-state and pulsed power supplies [2–6]. The former is usually used as a power source for the auxiliary heating system and operates continuously for several hours. The power supply will inevitably inject energy into the load due to frequent and sudden load reductions (called breakdown) [7]. However, due to the pricey and fragile load, this energy must be strictly limited. The latter usually provides a specific pulsed current

waveform for the fusion device, and the operating time is typically in the range of μs to ms . The output current of the power supply will generate a strong stray magnetic field that may cause components such as electromagnetic actuators in the power supply to fail [8]. As fusion devices and power supplies develop, the engineering complexity and control difficulty will increase further. More advanced and easily operated control frameworks are needed to facilitate the operation and control of the devices [9]. Therefore, the importance of research on fusion power supply technology is becoming increasingly prominent.

The following power technology research and applications have been carried out in recent years by the J-TEXT engineering team using the J-TEXT device, the International Thermonuclear Experimental Reactor (ITER) project, and the

* Author to whom any correspondence should be addressed.

China Fusion Engineering Test Reactor (CFETR): (1) a high-voltage power supply for an auxiliary heating system; (2) a breakdown protection device for an auxiliary heating power supply; (3) magnetic field compatibility; (4) a high-voltage pulsed power supply for a field-reversed configuration (FRC); (5) a large physics experimental facility control system. This paper summarizes the results of the past few years and suggests future research directions.

The high-voltage power supply for the auxiliary heating system has been a challenge for fusion engineering due to its characteristics of high voltage, high power, easy breakdown and quick shutdown. At present, there are two main types of power supplies: a pulse step modulation (PSM) power supply, and an inverter-type DC (ITDC) power supply. The PSM power supply has been successfully developed as the cathode power supply for the electron cyclotron resonance heating (ECRH) system of J-TEXT [10]. Its circuit scheme, queue-up control strategy and sub-module without voltage overshoot are presented. The ITDC power supply is planned for use as a 200 kV/25 A acceleration grid power supply (AGPS) for the CFETR prototype negative-ion neutral beam injection (N-NBI) system [11]. Its circuit scheme, low-voltage ripple strategy and main engineering design are demonstrated. The characteristics of both power supplies and future research directions are also discussed.

High-voltage power supplies for auxiliary heating often face the problem of load breakdown [12]. These particular loads are very sensitive to surge energy during breakdown. Protective switches and snubbers are two devices that are used to deal with this problem [13, 14]. We proposed the advanced chopper sub-module (ACSM) with voltage balancing capability and developed a 30 kV solid-state protective switch based on a silicon carbide metal-oxide-semiconductor field-effect transistor (SiC MOSFET). In addition, a new equivalent circuit model of the snubber is derived, which is close to the real experimental results. The design of the snubber for 200 kV AGPS is also mentioned.

The coil power supply usually operates with a high output current, and it will generate a high stray magnetic field (SMF) and lead to severe magnetic field interference (MFI) problems [8]. It is much more serious around the tokamak device and draws the attention of the ITER Organization [15]. At present, the magnetic field immunity test is the most efficient method to qualify the sensitive equipment under high SMF due to the lack of experience of MFI problems [8]. We proposed the optimization design method of the magnetic field generating coil [16], which is the key component of the test platform, and designed the test coils for J-TEXT and ITER, and also helped the Institute of Plasma Physics, Chinese Academy of Sciences (ASIPP) to complete the design of the test platform [17, 18]. In addition, the exploration of the failure of electromagnetic actuators [19, 20], which are the most sensitive to SMF, and their optimization [21] is briefly introduced.

In recent years, an experimental device for FRC has been under construction in Huazhong University of Science and Technology (HUST), and it is named HFRC (short for HUST-FRC). The pulsed power supply plays a significant role in the

formation of a high-performance FRC plasma [22]. Due to the high-voltage and low-load characteristics of the power supply and the requirement for low timing dispersibility on the discharge control, it leads to great challenges for the design and development of the power supply. We proposed new schemes and developed a high-voltage floating trigger and a high-voltage laminated busbar to solve these problems. The details of these two issues together with the development and test of the power supply will be briefly presented.

Experimental facilities like tokamaks often consist of many different types of power supplies. A control system that is adaptable and dependable is required to control the power supplies and numerous other kinds of instruments and devices. The Control system Framework for Experimental devices Toolkit (CFET) is a supervisory control and data acquisition (SCADA) software tool that is provided for control system building, which is fully designed based on Web technologies [9]. Compared to the traditional SCADA software tool, CFET has clear advantages in convenience and interoperability. HFRC chose CFET to build the control system to meet its requirements for real-time control. With this control system, a series of experiments have been finished in the past year.

The rest of this paper is organized as follows. In section 2, the scheme design and improved control strategy of the PSM power supply and ITDC power supply are presented. In section 3, an improved switching module based on SiC MOSFET and the circuit model and design of the snubber are introduced. In section 4, the design of the large-scale magnetic field generation coils for the immunity test and the failure analysis of electromagnetic actuators in an SMF are shown. In section 5, the design and development of the high-voltage pulsed power supply for HFRC are presented. In section 6, the CFET-based control system and its application in the HUST HFRC are described. Finally, section 7 summarizes this paper.

2. High-voltage power supply for auxiliary heating system

2.1. PSM power supply

PSM power supplies consist of many power supply modules connected in series at the output [23]. It is flexible, versatile and its output voltage is continuously adjustable over a wide range with high accuracy and low ripple [24, 25]. Due to the fact that the higher the output voltage, the more power modules are required, the most suitable voltage range of the PSM power supply is 100 kV and below.

2.1.1. Circuit scheme design. To power the electron gyron of the ECRH system, a 100 kV/60 A high-voltage power supply was built on the J-TEXT tokamak. The power supply is based on PSM technology [26], as shown in figure 1. The 100 MW pulse generator outputs an AC voltage of 6.3 kV/80 Hz. Four dry-type transformers with 36 secondary windings isolate the voltage of the generator and supply the 144 switching power supply (SPS) modules. Compared to

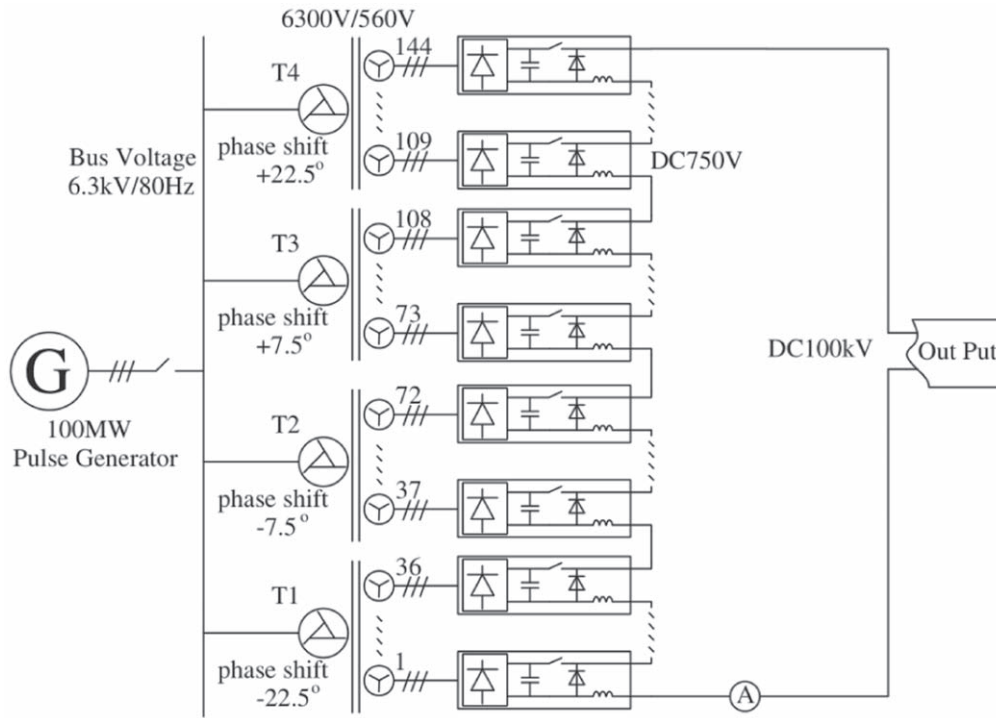


Figure 1. A schematic diagram of the PSM power supply. © [2014] IEEE. Reprinted, with permission, from [26].

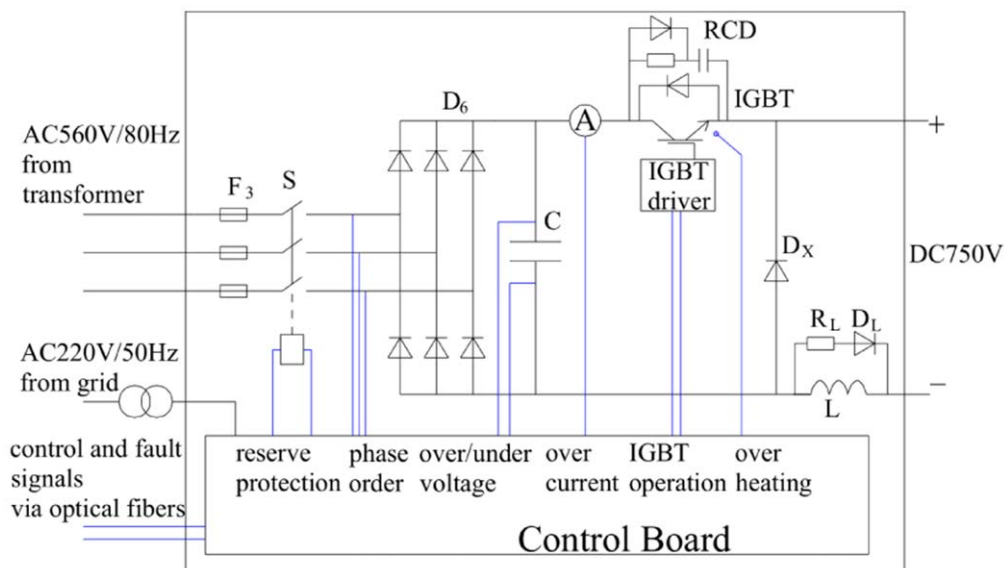


Figure 2. A single SPS circuit. © [2014] IEEE. Reprinted, with permission, from [26].

oil-immersed transformers, the dry-type transformer does not require frequent maintenance, has no fire safety hazards and has much less stray capacitance.

The scheme of a single SPS is shown in figure 2 [26]. In the SPS, a three-phase diode rectifier and filter capacitor will produce a 750 V DC voltage. The insulated gate bipolar transistor (IGBT) controls whether the module participates in the output of the power supply. The detailed design process of the SPS is described in [27]. A control system based on peripheral component interconnection (PCI) extensions for instrumentation (PXI) and a field-programmable gate array controller are

developed to provide switching signals and fault protection signals for each SPS. It has a protection response capability of up to 5 μ s for current faults and meets the ITER control, data access and communication (CODAC) standard [28].

2.1.2. Improved queue-up PSM control strategy. A PSM power supply generally uses phase-shifted pulse width modulation (PS-PWM) to control the output voltage of the power supply [29]. For PS-PWM, each SPS operates in PWM mode with the same switching frequency f_s (1 kHz) and duty cycle; the switching period is delayed sequentially between different

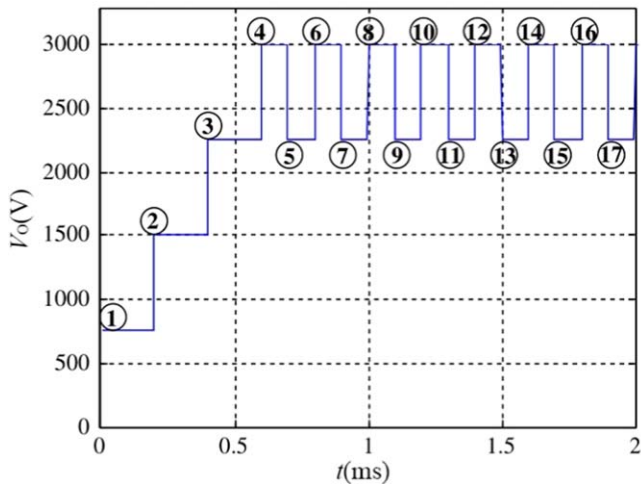


Figure 3. The working principle of the queue-up PSM technique [30] (2014). (Copyright Springer Science + Business Media New York 2014.) With permission from Springer.

SPSs. When the output voltage V_O of the PSM power supply needs to be changed, one cycle of the reference PWM signal must be passed, i.e. the regulation time of V_O is $1/f_S$.

To improve the response speed of the PSM power supply, a queue-up control strategy is proposed in [30]. The output voltage waveform can be computed using the known output voltage and switching frequency, as shown in figure 3. When there is a rising edge or falling edge of V_O , one SPS will turn on or turn off. All the SPSs are divided into two groups according to the on and off states, and are arranged by serial number. The regulation time of V_O is $1/f_{eq}$, which is much smaller than that of PS-PWM. The queue-up control strategy has been verified by experiments.

2.1.3. SPS module without voltage overshoot. Many loads of fusion high-voltage power supplies, such as electron cyclotrons and klystrons, are sensitive to voltage overshoot and short-circuit energy [31]. Overvoltage should be limited because it may cause or accelerate the damage to these loads over time [32]. The causes of voltage overshoot generation in PSM power supplies have been analyzed [33]. When the SPS is not yet outputting current, the capacitance voltage of the SPS is the peak value of the transformer line voltage. When the SPS is outputting current, the capacitance voltage will drop to the rated value.

To solve these problems, an SPS module structure that can suppress voltage overshoot was proposed, as shown in figure 4. Compared with the previous scheme, a soft-start resistor R_{soft} and switch S_2 are added. The specific circuit working process and parameter design are shown in [33]. The results show that the voltage overshoot suppression effect of the new module is significant, which can be reduced from 10.7% to 0.7%.

2.2. ITDC power supply

An ITDC power supply generally consists of two parts: a conversion system (CS), and a direct current generator (DCG)

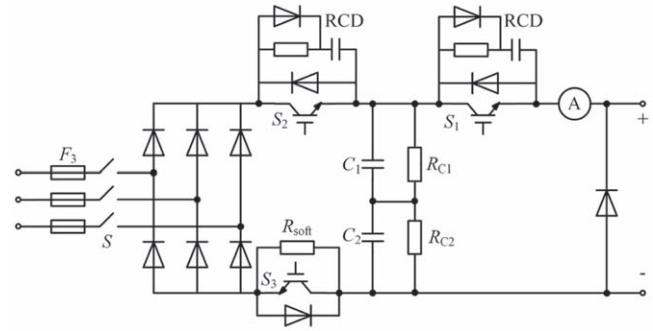


Figure 4. The SPS module circuit without voltage overshoot.

[34]. The CS consists of a rectifier and an inverter. The DCG consists of a step-up transformer, a high-voltage rectifier and a high-voltage filter.

The CFETR N-NBI system requires an AGPS with 1000 kV output voltage composed of five stages of 200 kV output in series. Due to the great engineering difficulties and the lack of development experience in China, there are plans to develop a single-stage 200 kV/25 A AGPS prototype first. It uses the ITDC scheme [35].

2.2.1. Circuit scheme design. The AGPS prototype with 200 kV is shown in figure 5 [34]. The rectifier of the CS uses a 12-pulse rectifier, which can provide two independent DC buses and reduce the reactive power and harmonic content of the grid. The inverter of the CS is a three-level scheme with neutral point clamping (3L-NPC). It creates lower voltage stress on the switching devices compared to the usual two-level scheme.

The step-up transformer (ratio 1:23.6) raises the AC voltage from the inverter of the CS and achieves electrical isolation. The high-voltage rectifier is a three-phase diode rectifier, consisting of a large number of diodes connected in series to achieve a high insulation voltage. The DCG does not contain any switching devices, which makes it much more reliable than the PSM scheme, especially when the power supply is under breakdown conditions [36].

The output current of each stage in the future 1 MV AGPS is about 75 A. To meet the demand of a larger capacity power supply, a new 5L-NPC/H multilevel converter scheme combining 3L-NPC and a cascaded H-bridge is proposed in [37], as shown in figure 6. This scheme has also been adopted by ABB and Tmeic, and its feasibility and reliability have been proven [38, 39]. Compared to the parallel 3L-NPC scheme, the 5L-NPC scheme retains the advantages of modular design, but without the need to consider the current balance of the switching devices. In addition, it has more numbers of levels for the output voltage, which reduces the harmonic content of the step-up transformer.

2.2.2. Engineering design of the inverter. Due to the fact that switching devices also have a significant impact on the inverter, detailed comparison and experimental analysis of different types of semiconductor power devices have been carried out [40]. Integrated gate commutated thyristors

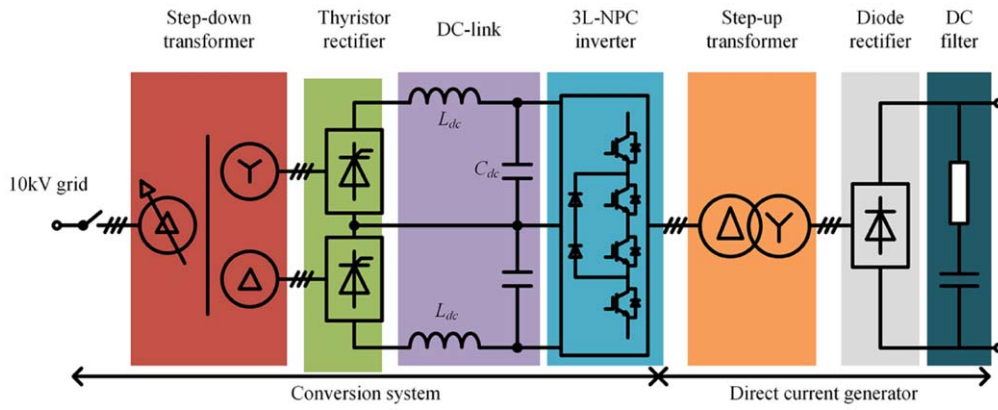


Figure 5. The circuit scheme of the 200 kV AGPS prototype. Reproduced from [34]. Copyright 2020 Hefei Institutes of Physical Science, Chinese Academy of Sciences and IOP Publishing. All rights reserved.

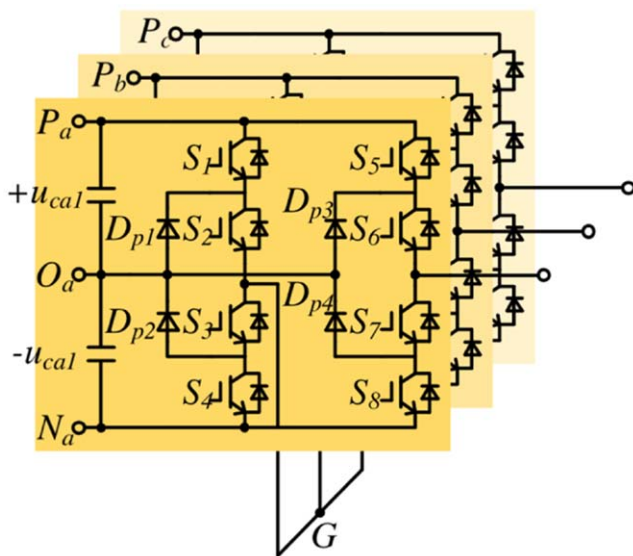


Figure 6. The 5L-NPC/H inverter topology. Reprinted from [37]. Copyright (2021), with permission from Elsevier.

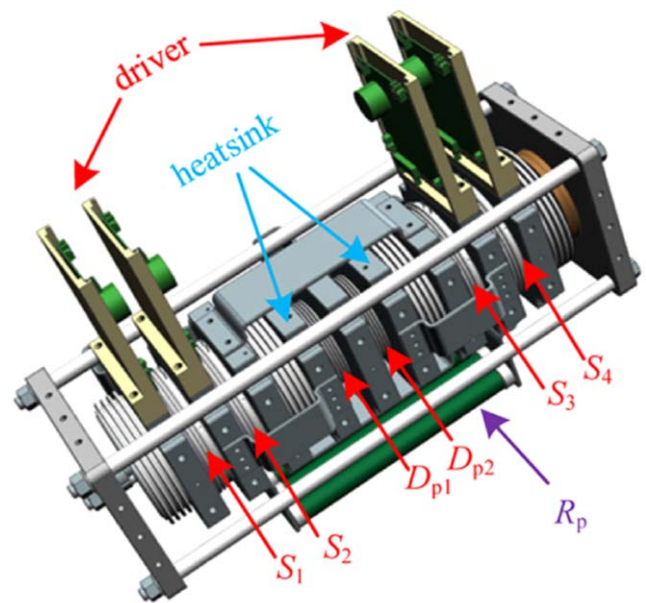


Figure 7. The structural design of one phase-leg of the inverter. Reprinted from [36]. Copyright (2019), with permission from Elsevier.

(IGCT) (5SHY35 L4520) from ABB and the injection enhanced gate transistor (IEGT) (ST1500GXH24) from Toshiba are identified as the most suitable switching devices. The detailed parameters of both are from their datasheets [41, 42]. As the inverter needs to turn off frequently and cut off a large current quickly when breakdown occurs, the IEGT is selected as the switching device of the inverter [40].

Figure 7 shows the phase-leg structure after several iterations of the design. The stray inductances are extracted by ANSYS/Q3D and the results are less than 400 nH. Moreover, the thermal simulation results show that the temperature of the IEGT and diode is lower than 50 °C. These indicate that the design of the phase-leg is reasonable [36].

2.2.3. Control method for low ripple output voltage. The ripple will increase significantly when the output voltage V_O of the AGPS is reduced [43]. The ripple cannot be reduced by increasing the inverter switching frequency due to the transformer heat rise. To reduce the short-circuit energy of

breakdown, the resistance-capacitance filter (RC filter) cannot be modified to improve the filtering effect. If the DC bus voltage V_{dc} remains constant and the output voltage is adjusted by the inverter duty ratio, this conventional control strategy will not be able to meet the ripple requirements [44].

Zhang *et al* analyzed the DCG equivalent circuit of the AGPS in depth and found that the ripple reaches the minimum value when V_{dc} and V_O satisfy [45]:

$$V_O = 3nV_{dc} \tag{1}$$

where n is the turn ratio of the step-up transformer. The duty ratio d_{min} corresponds to the minimum ripple and can be obtained from equation (1). Accordingly, the combined control strategy of the DC bus voltage and the duty ratio is proposed, as shown in figure 8. The control strategy is verified by simulation and experiment [45]. The ripple of the

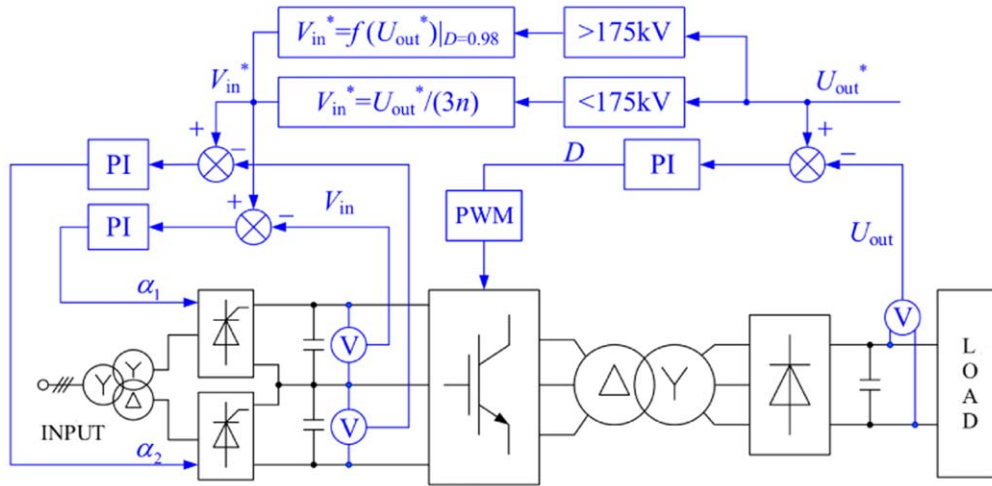


Figure 8. The combined control strategy. © [2019] IEEE. Reprinted, with permission, from [45].

output voltage decreases from 15.27% to 1.43%, and the ripple requirement of the AGPS can be satisfied.

For the inverter scheme of the 5L-NPC/H, Wang *et al* derived a mathematical model [46]. Based on this model, the control strategy of the AGPS with high accuracy and the low ripple output voltage is studied. The control strategy is verified by simulation and also meets the ripple design requirements [47].

2.2.4. Voltage balance of a large number of series diodes. In the 200 kV AGPS prototype, both static and dynamic voltage balances of the diodes are important because V_O will change rapidly under breakdown conditions. Because of the size of the rectifier ($4.4 \text{ m} \times 2.5 \text{ m} \times 4.7 \text{ m}$), the stray capacitance C_p of each diode cannot be ignored. It causes significant voltage unevenness in the series diode, even though each diode has been connected in parallel with a snubber circuit and a balancing resistor.

Yang *et al* proposed a non-isoparametric snubber circuit method that considered the stray capacitance of the diodes [48]. To achieve the voltage balance, each diode has a damping resistor R_d , a snubber capacitor C_s and a static voltage balancing resistor R_b . When these parameters and C_p satisfy equation (2), the circuit model can be simplified, where the subscript j indicates the order number of a certain diode:

$$\frac{\omega_{\text{inv}} R_{dj} C_{sj} C_{pj}}{C_{sj} + C_{pj}} \ll 1. \quad (2)$$

The new snubber capacitance C_{Dj} and damping resistance R_{Dj} can be calculated according to the different C_p so that these two parameters are equal for each diode. With this method, the dynamic voltage equalization factor of the diode rectifier can be increased from 0.80 to 0.99.

2.3. Summary and future research directions

The PSM and the ITDC power supplies are two typical high-voltage power supply schemes for auxiliary heating systems. PSM power supplies have the characteristics of fast response, high accuracy, low ripple and small voltage overshoot due to recent research and development. They can be used for applications up to 100 kV. The ITDC power supply is more suitable for applications above 100 kV than the PSM power supply. It is more reliable than the PSM power supply. As a result of the research in recent years, the ripple suppression strategy has been perfected, and the output voltage ripple will no longer be a significant problem.

However, there are still some problems or things that can be improved. The analysis and purposeful design during breakdown conditions are very important for both power supplies, but they are still missing. In addition, for PSM power supplies, the dynamic voltage balancing of the SPS under breakdown conditions will be the main factor constraint to increasing the output voltage, which is also worth studying in the future; for the ITDC power supply, the dynamic response capability needs to be improved to meet possible future demands.

3. Breakdown protection device for auxiliary heating system

ECRH, NBI, and low hybrid current drive systems are all fusion devices that are used for auxiliary heating of the plasma. The cyclotron, ion source and klystron act as the loads of the high-voltage power supplies, driven and powered by the high-voltage power supply. However, due to breakdown conditions, they will be subjected to the energy injected by the power supply and the energy from the stray capacitance of the power supply. These energies should be strictly limited to protect these expensive and precise loads [49, 50]. The addition of protective switches and snubbers between the

power supply and the load are two ways to effectively reduce the energy [51, 52].

3.1. High-voltage protection switch

Protective switches can be divided into two types: mechanical switches, and solid-state switches. Mechanical switches have high-voltage ratings, but slow response times, low switching frequency, a short lifetime and arcing [53]. To cut the connection between power and load within a few μs for suppression of short-circuit energy, solid-state switches with fast shutdown capability and no arcing are an attractive solution [54]. However, there are still many problems with protective switches in terms of voltage balancing and switching speed [55]. How to develop fast and reliable protective switches is still a critical issue.

3.1.1. Comparison and selection of switching devices. Since the output current of high-voltage power supplies is generally within tens of amperes, both IGBTs and MOSFETs can be used as semiconductor devices for solid-state switches. MOSFETs do not have conductance modulation effects, which have better turn-off performance but higher on-resistance than IGBTs [56]. The development of SiC MOSFETs has matured in recent years. It has a higher blocking voltage, lower switching losses and a higher operating temperature [57]. Therefore, it has received a lot of attention and will be considered a competitive switching device for high-voltage power protection switches [58].

Double-pulse tests were conducted on a SiC MOSFET (C2M0080170P) and a Si IGBT (IXYH16N170C), both with rated parameters of 1400 V/40 A, respectively, to further compare the performance of the two semiconductor devices [59]. The results show that solid-state switches made up of SiC MOSFETs have lower turn-off loss and faster turn-off speed if their peak voltages are within the allowable range.

3.1.2. Advanced chopper sub-module. The faster turn-off speed of SiC MOSFETs can easily cause voltage imbalance between the series devices during the turn-off process. An improved switching module, known as the ACSM, is proposed to enhance the voltage balance of SiC MOSFETs without reducing switching speed, as shown in figure 9. The operating process and parameter design are described in [60]. Compared to the resistance-capacitance-diode snubber (RCD snubber), it has fewer devices; therefore, the reliability of the circuit can be guaranteed. However, the ACSM can still maintain a fast turn-off speed.

Figure 10 shows the experimental results of two series-connected ACSMs in the simulation of the breakdown of a 1.5 kV supply. The solid-state switch has a turn-off time of 23.6 ns, indicating that the ACSM does not slow down the turn-off speed of the SiC MOSFET and voltage balancing can be achieved. Based on this, a 40 kV/25 A solid-state switch consisting of 64 ACSM modules connected in series was developed. It has been tested on a 30 kV cathode power supply of the ECRH system [60].

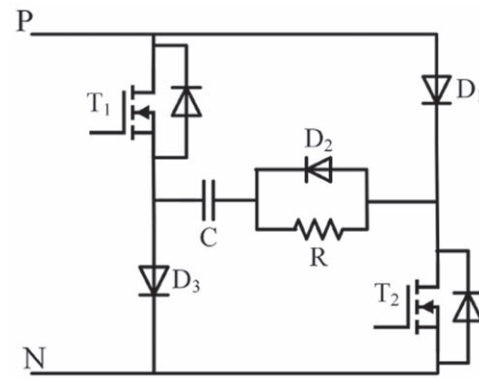


Figure 9. The topology of the proposed ACSM. Reprinted from [60]. Copyright 2021 Author(s), with the permission of AIP Publishing.

3.2. Snubber for short-circuit energy suppression

A snubber, a device installed between the power supply and the load, is another way to suppress short-circuit energy. It generally consists of a toroidal core and a winding wrapped around the core, which may be connected to additional power supplies, resistors and other components. The equivalent magnetization inductance of the snubber can suppress the current rise rate and convert some short-circuit energy into its core losses [61].

3.2.1. Equivalent circuit model of the snubber. The operating process of the snubber has nonlinear and time-varying characteristics. It brings the difficulty of solving the nonlinear problem [62]. Therefore, a suitable equivalent circuit model makes the equivalent circuit of the snubber more realistic, and an improved equivalent circuit model is helpful for the design of the snubber and the analysis of the power supply.

To make the equivalent circuit of the snubber more realistic, an improved equivalent circuit model is proposed in [62]. In this circuit model, the magnetization inductance when the snubber voltage V_S is less than 0 can also be determined by a specific expression. This is what was not mentioned in the previous study. To verify the new model, the snubber during short-circuit discharge of the capacitor C_a with initial voltage V_C was simulated and compared with experimental results. It is shown that the circuit model is highly consistent with the experimental waveforms, indicating that the new equivalent circuit model can basically emulate the operating process of the snubber.

3.2.2. Snubber analysis and design of AGPS. For the AGPS, the diode in the high-voltage rectifier in the off state is connected in parallel with C_a . To suppress the transient current of the diode during the breakdown, a series resistor R_{dr} is added to the branch of the diode. Reference [63] analyzed this circuit with or without the diode and with different R_{dr} . It was found that the diode does not affect the peak value of i_A , but prolongs the decay time of i_A .

The magnetic tape ought to be sufficiently thick to prevent saturation of the snubber's core, but this is constrained by material properties and manufacturing methods. One

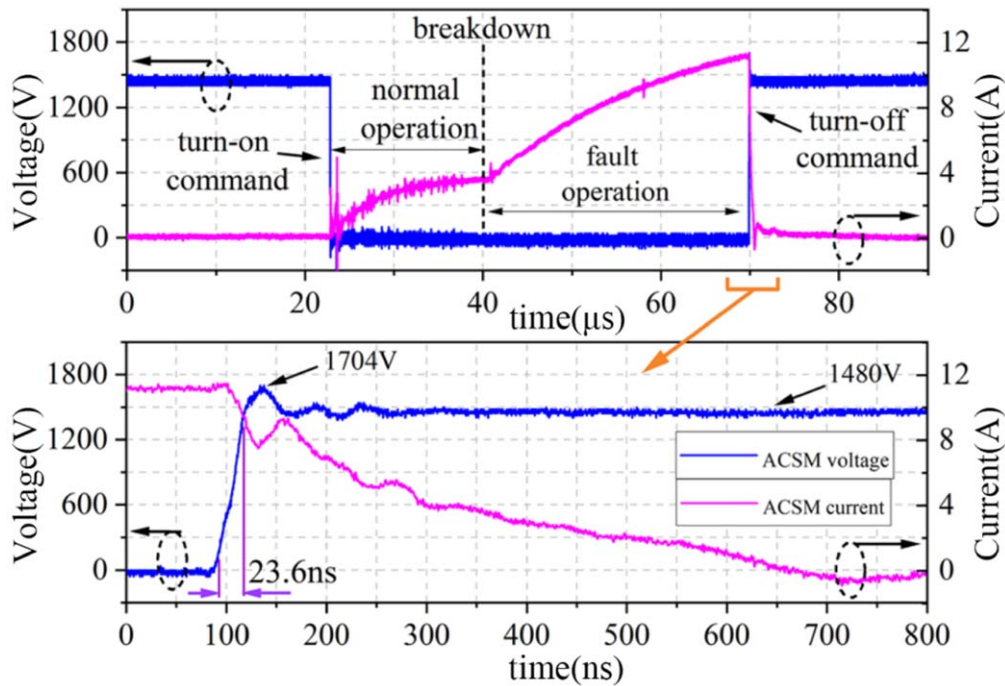


Figure 10. Experiments with two ACSMs in series. Reprinted from [60]. Copyright 2021 Author(s), with the permission of AIP Publishing.

solution is to connect a resistor R_S to the winding of the snubber. Simulations and experiments with several different R_S are carried out and the design of R_S is described in [63].

The final AGPS snubber design is confirmed through several design iterative processes, and the relevant parameters are shown in [63].

3.3. Summary and future work arrangements

The energy released to the load by the auxiliary heating power supply can be suppressed by two methods, which are solid-state switches and snubbers. Solid-state switches suppress the energy that the power supply continues to inject into the load after breakdown occurs and are suitable for high-voltage power supplies up to 100 kV. Snubbers can be used in any high-voltage power supply by suppressing not only the energy injected from the power supply but also the energy stored in the power supply stray capacitor. Higher-voltage testing of the solid-state switch will be considered and put into practical use in the future. The development of snubbers and further research will also be conducted in the future.

4. Magnetic field compatibility

Due to the high SMF generated by the tokamak device [15] and its coil power supply [8], the electrical and electronic components mounted in the high SMF environment will suffer severe MFI problems. The ITER Organization found that electromagnetic relays, contactors, programmable transducers, converters and power supply modules will fail in an SMF with strength within 25 mT [64–66]. As these components are widely used in the auxiliary systems of tokamak

devices, the MFI problem will be a great threat to the reliable operation of tokamak devices.

The study of the MFI problem mainly includes two aspects, namely a magnetic field immunity test, and failure analysis and optimization. The former attempts to quantify the failure threshold of sensitive equipment to verify whether it will operate normally in an SMF, while the latter attempts to reveal the failure mechanism of a sensitive component and find an optimization solution.

4.1. Magnetic field immunity test platform

The ITER Organization requires a mandatory qualification test for all the electrical and electronic devices where the SMF is over 5 mT, and only the devices that pass the test will be accepted [67]. A magnetic field immunity test platform is an essential facility to qualify the sensitive equipment in the presence of MFI. It usually consists of a magnetic field generation coil, a power supply, a control and data acquisition system and other auxiliary systems, of which the magnetic field generation coil is the most important component. Due to the large size of the tested equipment and the high SMF, it brings a great challenge to the design and fabrication of the coil.

In the immunity test of a power frequency magnetic field specified in IEC 61000-4-8 [68] and a DC magnetic field specified in DOD-STD-1399 [69], a single turn coil or Helmholtz coil pair is usually used to generate the test field as the specified test level is low. However, it is not the best choice as the coil design has not resulted from a proper definition of the test field. In 2018, a complete definition of the test field was first given, which adopts three parameters to characterize the test field. Based on the definition, an improved two-coil configuration together with several simple

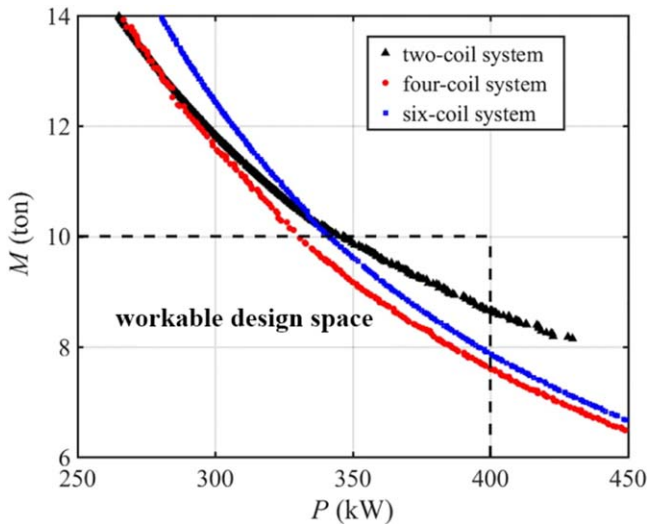
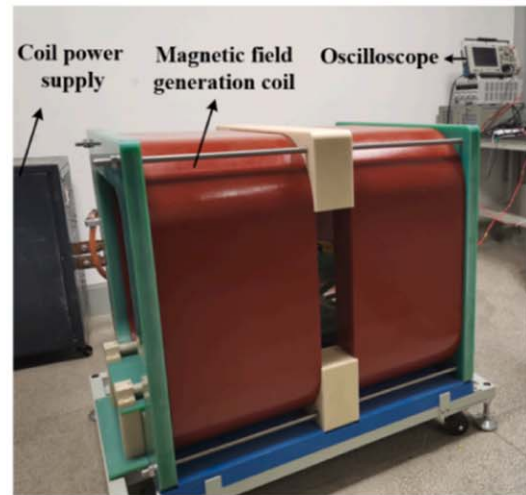


Figure 11. Pareto-optimal fronts of different coil systems (power loss versus conductor mass) [17]. John Wiley & Sons. Copyright 2022 The Authors.

formulae for the fast design was proposed [16]. Its performance in generating the test field is better than the commonly used Helmholtz coil. Improved multi-coil configurations were also proposed [70, 71]. As these improved coils are obtained from the line-current assumption, they are valid if the cross-section of the coil is small, and the field strength is only within several tens of mT. If a test field of strength over hundreds of mT is needed, more work will be required to obtain a further optimized design.

As the SMF around the ITER tokamak is over hundreds of mT, and the size of the largest sensitive equipment is over 1 m [67], a large-scale high-intensity test coil is needed. This indicates that the test coil will have a high weight and high operation power. How to balance the weight and the power becomes the key point in the design of a large-scale test coil. A multi-object optimization method based on a non-dominated sorting genetic algorithm (NSGA-II) is proposed to solve this problem in [17]. In the proposed method, the weight and power are treated as the optimization object, the structure parameters are treated as the variables, the characteristic parameters of the test field are treated as the constraints, and a Pareto-front, as shown in figure 11, is obtained. This method has been successfully applied in the ITER test coil. Moreover, we found that adding a magnetically shielded room will further improve the coil performance [72].

By now, a small test platform was established at J-TEXT, as shown in figure 12(a). It can generate a magnetic field over 200 mT in a cubic space with a side length of 0.3 m, and the field inhomogeneity is only 1.05 [73]. A 2.1 m test platform was built at ASIPP, as shown in figure 12(b). It has a 120 mT magnetic field and the field inhomogeneity is 1.2 [18]. We have also designed a test coil for the ITER Organization for the qualification test, as shown in figure 12(c). The test zone size is 1 m, the field strength is 275 mT and the field inhomogeneity is 1.05 [17]. All three coils are cooled by water due to the high operating power.



(a)



(b)



(c)

Figure 12. Test coils built at J-TEXT, ASIPP and ITER. (a) The 0.3 m/200 mT test coil at J-TEXT. Reprinted from [73]. Copyright (2022), with permission from Elsevier. (b) The 2.1 m/120 mT test coil at ASIPP. Reprinted from [18]. Copyright (2021), with permission from Elsevier. (c) The 1 m/275 mT test coil at ITER. [17] John Wiley & Sons. Copyright 2022 The Authors.

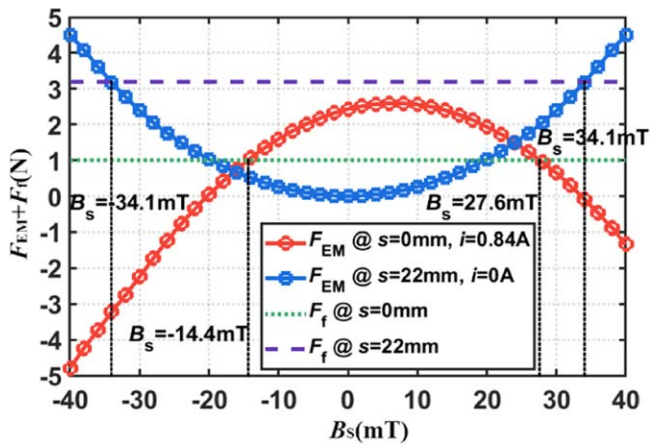


Figure 13. Calculated total electromagnetic force (F_{EM}) and spring force (F_f) exerted on the armature under different SMFs. Reproduced from [20]. Copyright 2022 Hefei Institutes of Physical Science, Chinese Academy of Sciences and IOP Publishing. All rights reserved.

To satisfy the qualification test of the largest equipment at the highest level in the future, a test coil that can generate a magnetic field over 400 mT or even higher in a cubic space with a side length of 2.1 m will be needed. The design and fabrication of such a huge test coil will be more challenging.

4.2. Failure of linear electromagnetic actuators (LEA)

MFI can be roughly divided into three types. The first relates to the elements which are based on the magnetic effect, like the Hall effect and magneto-resistive effect. The second relates to static devices which contain a magnetic core, like inductors and transformers. The last relates to the dynamic devices which contain magnetic materials, like electromagnetic actuators and motors. The tests carried out by the ITER Organization show that electromagnetic actuators, like relays and contactors, are among the most sensitive devices to an SMF [65, 66]. The influence of an SMF on LEAs is under exploration in J-TEXT, and its recent advances are briefly introduced below.

Finite element analysis of piston-type and plate-type LEAs shows that the additional force exerted on the armature leads to the failure of the LEAs, and the failure mode depends on the LEA structure [19]. The piston-type will refuse to act when the LEA is energized, while the plate-type LEA will malfunction, even if no driving current is applied. Besides, both types will fail to return to the initial position during the opening process if the SMF is strong enough. In the presence of the excitation magnetic field, the direction of the SMF also has an impact, with a negative SMF having a greater impact on the LEA than a positive SMF. The analysis quantifies the failure threshold of the LEA under the rated condition, which is -14.4 mT and 27.6 mT in the negative and positive directions for the piston-type LEA, as shown in figure 13 [20], and it is verified by experimental tests conducted on the small platform, as shown in figure 12(a).

A multi-physics analysis model involving a magnetic field, electric circuit and mechanical motion is also proposed to study the dynamic performance of a piston-type LEA in the SMF. The analysis further verifies the conclusion that the

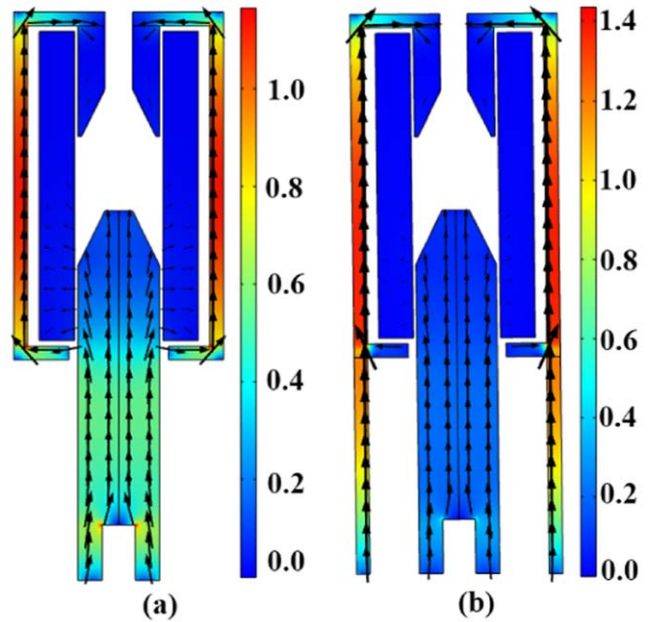


Figure 14. The magnetic field distribution in the iron core: (a) the original magnetic field, and (b) the improved magnetic field. Reprinted from [73]. Copyright (2022), with permission from Elsevier.

influence of an SMF on the LEA is mainly contributed by the additional force exerted on the armature. The analysis also shows that the action time of the LEA has a positive correlation with the SMF strength within the failure threshold during the closing process. However, a negative SMF will speed up the armature return, while a positive SMF will impede it during the opening process.

Increasing the driving voltage can improve the immunity of the piston-type LEA against an SMF, but it will also increase the driving power, and may lead to a severe bounce. As the effect of the SMF gets weaker when the armature moves towards the contact point, a voltage-doubling circuit based on a pre-charged capacitor is proposed in [20]. The increased driving voltage ensures the successful action of the LEA under an SMF at the initial stage. As the armature moves, the voltage decreases as the capacitor discharges, and this will result in a low collision velocity.

The immunity of the LEA against an SMF can also be enhanced by optimizing its structure. An optimized LEA structure, by simply adding two small iron legs, as shown in figure 14, is proposed in [73]. The iron legs change the magnetic field distribution in the LEA, and significantly reduce the MFI of the LEA. Compared with the original LEA, the optimized LEA will not fail in a positive SMF and its failure threshold in a negative SMF is increased by 63%. Moreover, this method shows higher effectiveness than conventional magnetic shielding, with 40% of the material costs and considerably fewer space occupations to achieve the same failure threshold.

4.3. Summary and future work arrangements

The MFI problem is a great threat to the reliable operation of the tokamak device. However, it was usually overlooked until

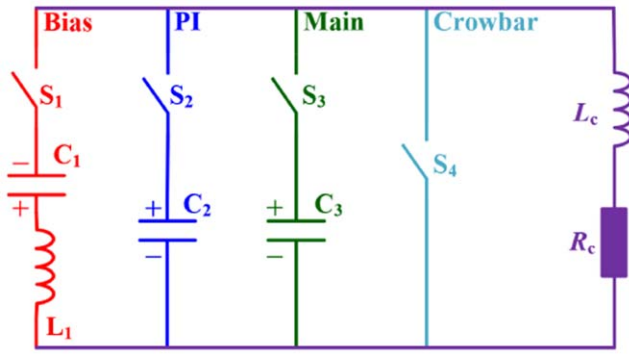


Figure 15. The topology of the HFRC high-voltage pulsed power supply.

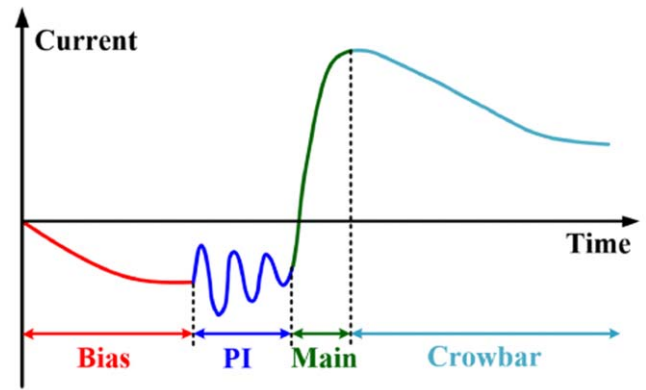


Figure 16. The typical current waveform of the high-voltage pulsed power supply. Reprinted from [22]. Copyright (2022), with permission from Elsevier.

the ITER Organization turned its attention to it. The successful building of these test platforms enables the qualification test of large equipment under high test levels and the exploration of MFI problems. Besides, a lot of experience has been accumulated for the design and development of a larger test platform with a higher test ability in the future.

The study of the LEA shows that the additional force exerted on the armature leads to the delay and even failure of the LEA in an SMF. Optimizing the driving circuit and iron core structure of the LEA will certainly increase its immunity against an SMF. However, this may also lead to a higher collision velocity and bounce problems. Intelligent control is needed to ensure the successful action as well as the soft landing of the LEA in this situation, and this will be the work in the next step. Moreover, there are plans to investigate and improve other kinds of electromagnetic actuators, such as planar and rotary actuators, as well as power modules.

5. High-voltage pulsed power supply for FRC

The high-voltage pulsed power supply is used to feed the θ -pinch coils for HFRC. The FRC plasma formation based on θ -pinch coils can be divided into four stages, namely applying a bias field, pre-ionization, field reversal and equilibrium. The pulsed power supply adopts the typical topology, as shown in figure 15, which contains four branches, namely bias, pre-ionization (PI), main and crowbar, and each corresponds to a formation stage [74]. If the switches S_1 – S_4 are triggered in sequence, a special current waveform, as shown in figure 16, will be generated in the θ -pinch coils for the FRC plasma formation [22]. The bias field is designed at 0.16 T, the ringing frequency of the PI branch is about 125 kHz, the magnitude of the main field is 0.5 T and its rising time is within 5 μ s. This results in the highest voltage at 40 kV and current at about 70 kA of the power supply.

5.1. Design of high-voltage floating trigger

Due to the high voltage and large current, hydrogen thyratrons are adopted as the switches in the power supply. However, the reliable triggering of the hydrogen thyatron is

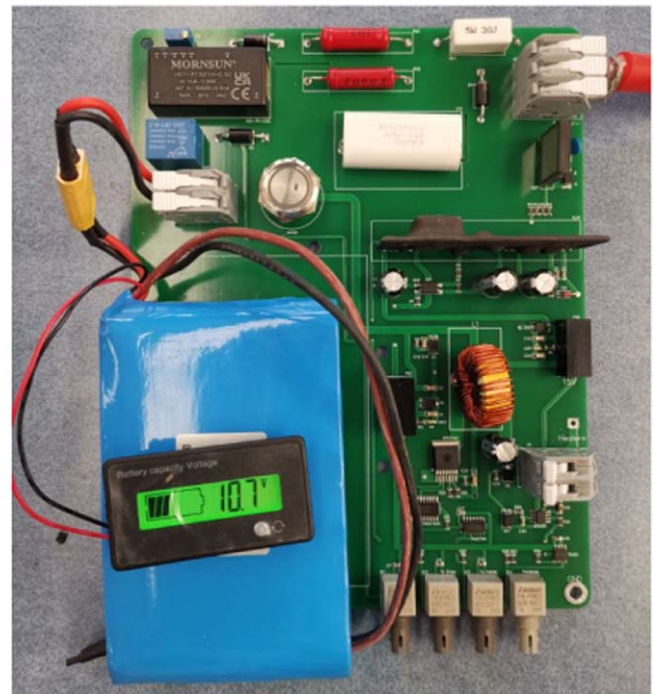


Figure 17. The trigger of the hydrogen thyatron.

relatively complex, which requires a heating circuit with 5 V voltage and a pulse generating circuit with 10 kV voltage. Thus, two high-voltage isolation transformers are needed [75]. However, the high-voltage isolation transformers will occupy a lot of space and increase the cost.

A high-voltage floating trigger, as shown in figure 17, has been developed to save space. The isolation transformers are turned off in the design, and the trigger operates in a floating state. The trigger is powered by a lithium battery, and the control signals are fed through optical fibers. The pulse generating circuit uses a high-voltage IGBT as the primary switch, which improves the switching speed and reliability. Experiments show that the trigger can work stably under a

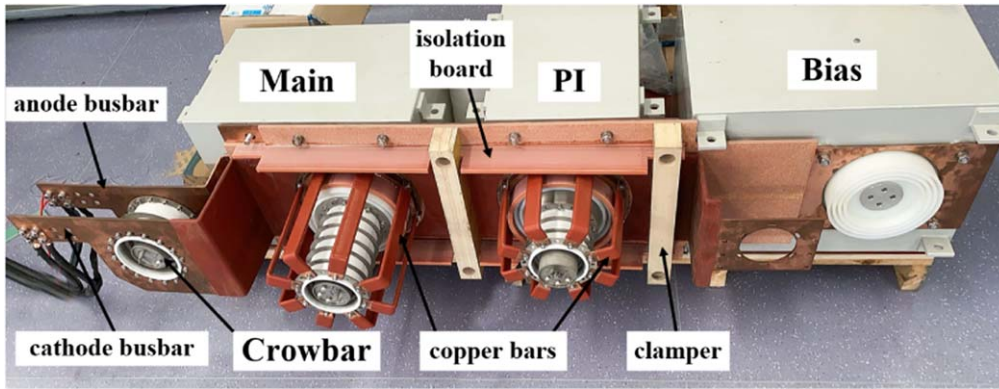


Figure 18. The prototype of the laminated busbar.

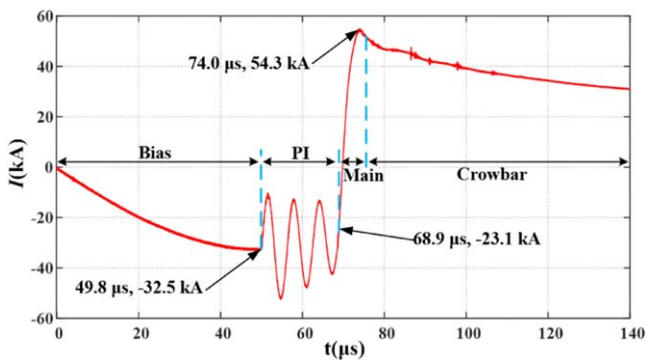


Figure 19. The output current waveform of the pulsed power supply. Reprinted from [22]. Copyright (2022), with permission from Elsevier.

high floating voltage of 35 kV with a voltage rising rate of about 12 kV/ μ s, and the total jitter time is less than 60 ns.

5.2. Design of high-voltage laminated busbar

As the load inductance of the power supply is about 1 μ H, the stray inductance of the power supply should be kept as low as possible. Therefore, a busbar with low stray inductance and high withstand voltage is needed.

A high-voltage laminated busbar, as shown in figure 18, has been developed. The laminated busbar mainly consists of a cathode busbar, an anode busbar, an isolation board, several clammers and connecting copper bars. The busbar's stray inductances are greatly reduced due to the proximity of the cathode and anode busbars. As a result, the power supply's output current and ringing frequency can be increased. Moreover, the insulation ability of the busbar is also improved due to its special insulating treatment. Experimental tests show that the busbar can withstand a steady-state voltage at 40 kV, and the output current and ringing frequency are both increased by over 10% with respect to conventional designs.

5.3. Integration and test

To date, the pulsed power supply of the HFRC has been installed and the commissioning is underway. Many repeated tests have

been conducted, and the results show that the pulsed power supply can operate stably. Figure 19 shows the current waveform of the pulsed power supply, where the bias, PI and main capacitor are charged to -20 kV, 28 kV and 34 kV, respectively. The ringing frequency of the PI branch is about 125 kHz, and the peak current of the main branch reaches 54.3 kA.

5.4. Summary and future work arrangements

The design of the hydrogen thyatron trigger and laminated busbar greatly improves the performance of the pulsed power supply and makes it possible to obtain a high-parameter FRC plasma. In the following step, work will be carried out to further enhance the pulsed power supply's operational parameters and reliability. At first, the output voltage will double when two power supply modules are connected in series, as shown in figure 15, requiring additional engineering efforts. As the PI branch and main branch are directly connected in parallel, severe oscillation will occur, and it will limit the operational parameters of the power supply. Decoupling these two branches will be the second approach to improve the performance of the power supply.

6. Large physics experimental facility control system

6.1. Development of control system framework for experimental device toolkit

The deployment of the control system is necessary for the operation of large-scale experimental facilities. A control system framework is needed to make the development of the control system a manageable task. The experimental physics and industrial control system (EPICS) framework is the most widely used control system framework [76, 77]. It was widely accepted by the accelerator community as well as chosen by ITER. But it does have some drawbacks, as it was developed a long time ago and was mainly focused on performance.

As computers become much more powerful, the focus is shifted to interoperability. Interoperability enables the control system of an experimental facility to develop fast. It also allows the control system to be modified without difficulty, making the facility more flexible. We proposed an abstract

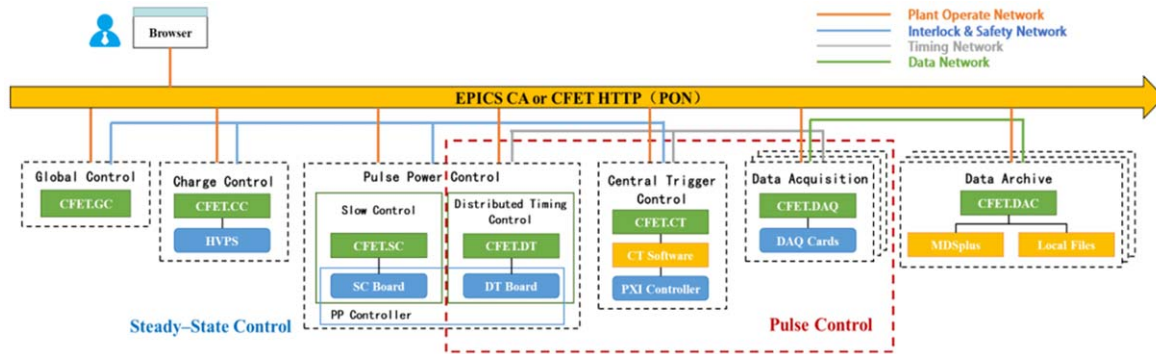


Figure 20. The overall structure of the whole system. Reprinted from [79]. Copyright (2022), with permission from Elsevier.

model for the control system and a control system framework called the CFET that uses web technology to build a control system.

The CFET framework is based on Web technologies which are almost supported by all types of devices. The CFET has the advantages of strong abstraction, a simplified framework and a transparent protocol. Based on Web technologies and Representational State Transfer (REST) design, the CFET is highly flexible and interoperable with low platform dependencies. Under the CFET abstraction framework, everything in the control system is a resource. The access resources can be classified into five types: Thing, Status, Config, Method and Event [78].

The main communication module of the CFET uses the hyper text transfer protocol (HTTP) protocol of the RESTful architecture as the basic transmission and communication protocol. Considering that EPICS Channel Access (CA) is the most commonly used communication protocol in the accelerator and fusion community, the CFET framework supports the mutual conversion between the EPICS CA protocol and the CFET communication protocol. The CFET communication module also supports Message Queuing Telemetry Transport and WebSocket. Since different control logics have different requirements for the human-machine interface, the CFET provides a user interface (UI) component library. It is a human-machine interface (HMI) editor. Users can build their own operation interface and generate the corresponding URL through the graphical interface operation.

6.2. Application on HUST-FRC fusion device

HFRC is composed of different devices and instruments. Each device has its own independent control logic and process. It is very important to coordinate and control many devices to make them operate safely and orderly as a whole system. HFRC uses the CFET as a development tool for control systems building. The HFRC central control system is composed of various subsystems divided by function and a group of control system networks.

The HFRC central control system architecture adopts the design of micro-services, and each subsystem works as an individual unit [79]. Every part enclosed by a black dotted line, as shown in figure 20, is a subsystem [79]. The green

part of the subsystem represents the software developed based on the CFET framework according to the functional requirements, and the blue part represents the hardware it controls. The HFRC central control system also includes a network structure. Subsystems are connected to each other through these communication networks, and they can use the services of other subsystems by accessing a specific control system network according to their own needs [80].

As shown in figure 21, the operator can easily control the entire experiment using the Web browser-based HFRC Global control system UI. The CFET-provided graphical components, such as the status light, wave and video player, allow for detailed monitoring of the experiment’s current status. Furthermore, each part of this dashboard can be constructed as one wishes.

After setting the parameter or turning the on/off switch by the Web UI, the experiment status will transfer under a certain control flow. The state machine of the HFRC Global control system is shown in figure 22 [79]. The operator can press start to make the system transfer into preparation status. In every step of the preparation status, one can press abort to stop and every subsystem returns to the idle state.

At present, the HFRC control system has been running stably for one year, and the relevant experiments have achieved preliminary results. The HFRC control system will continue to provide support for further experiments.

6.3. Summary and future work arrangements

For large experimental facilities, a flexible control system is the key to integrating various large numbers of devices, especially for numerous power supplies. We have developed the CFET control system framework for large experiment facilities, with the focus on interoperability. It works with industry standard Web technology, can run on almost any device and is easy to integrate with other control systems. The HFRC control system is developed based on the CFET framework. It has integrated more than 40 different types of power supplies and many other devices, and works reliably. In the future, the development focus of the CFET control system framework will be on the addition of more UI widgets and the addition of more support for different hardware

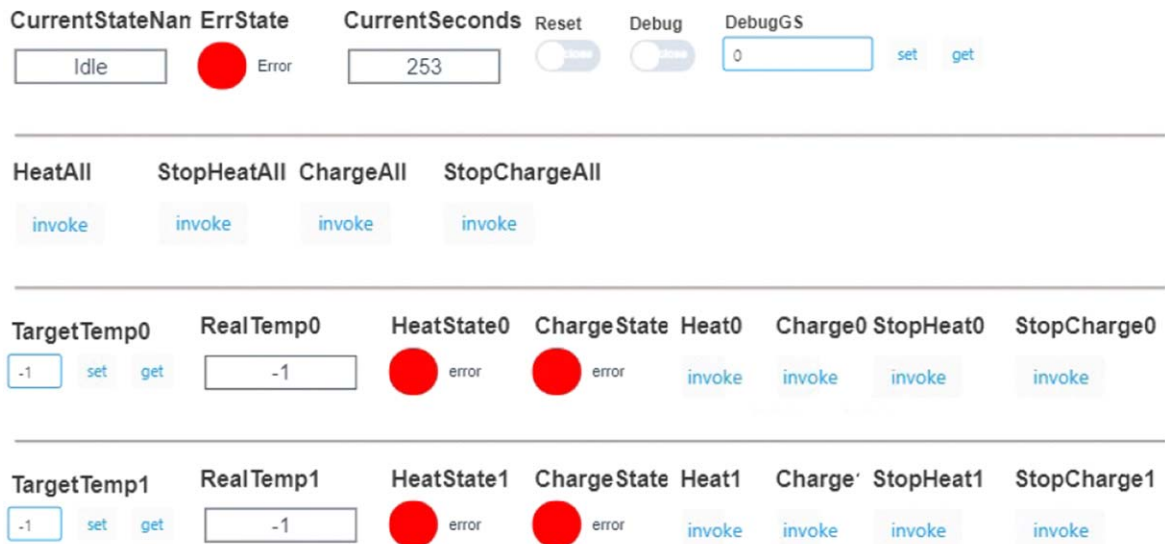


Figure 21. The UI of the Global control system.

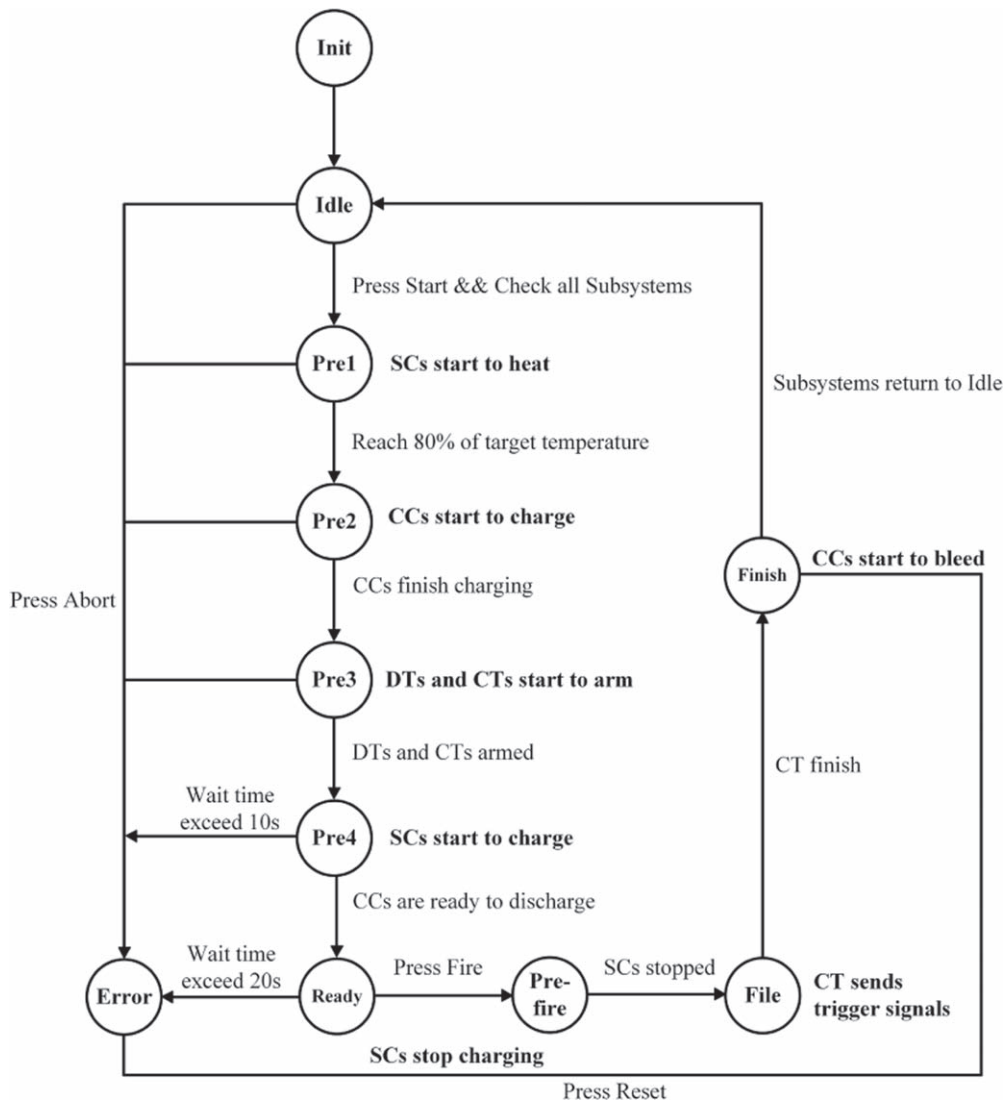


Figure 22. The state machine of the Global control system. Reprinted from [79]. Copyright (2022), with permission from Elsevier.

devices; integration with EPICS is also a very important feature to be improved.

7. Conclusions

This paper presents the fusion power supply advances at J-TEXT, including the following aspects:

- (1) The scheme design and improved control strategy of the PSM power supply for the hundred kV voltage level and ITDC power supply for the MV voltage level have been proposed and applied separately to the 100 kV/60 A cathode power supply for the J-TEXT ECRH system and the 200 kV/25 A AGPS for the CFETR prototype N-NBI system.
- (2) An improved switching module based on a SiC MOS-FET has been proposed and a 40 kV/25 A solid-state switch consisting of 64 ACSM modules connected in series has been developed. In addition, the optimized circuit model of the snubber has been presented and used as the basis for snubber analysis and design of the AGPS. The research of the protective switches and snubbers provides a solution for breakdown protection for an auxiliary heating power supply.
- (3) An optimization design method of the large-scale high-intensity magnetic field generating coils for the magnetic field immunity test is proposed, and it is successfully applied in the design of the test coils for J-TEXT and ITER, and helps ASIPP to complete the design of the test platform. In addition, failure analysis of an LEA under an SMF is performed, with several valuable improvements proposed, and this lays a foundation for the study of other similar devices that are sensitive to SMFs.
- (4) A high-voltage floating hydrogen thyatron trigger has been developed, and it increases the integration level and the control accuracy of the pulsed power supply of HFRC. Moreover, the performance of the power supply is also improved with the development of the high-voltage laminated busbar.
- (5) To meet the requirements of real-time control, strong interoperability and user-friendly, the CFET is chosen as the core to implement the HFRC control system. Compared to the traditional SCADA software tool, the CFET has clear advantages of convenience and interoperability, because it is designed with industrial standard Web technology and aimed at interoperability. Now, a control system based on the CFET has been deployed for HFRC, and a series of experiments have been successfully finished.

In this process, some engineering technology and experience have been accumulated, a series of improved schemes have been put forward and a group of scientific research staff with engineering construction capabilities have been cultivated and trained. In the future, the J-TEXT engineering team will continue to delve into the research of fusion

power sources, will propose more innovative improvements and will complete the development and experiments of various prototypes.

Acknowledgments

The authors would like to thank all the members of the J-TEXT engineering team for their excellent work and the other members of the J-TEXT team for their support. This work was supported by the National Key Research and Development Program of China (Nos. 2017YFE0300104 and 2017YFE0301803) and National Natural Science Foundation of China (No. 51821005).

ORCID iDs

Rumeng WANG (王如梦)  <https://orcid.org/0000-0001-6282-2075>

References

- [1] Tobar H *et al* 2017 *IEEE Trans. Plasma Sci.* **45** 162
- [2] Singh M J 2016 *IEEE Trans. Plasma Sci.* **44** 1514
- [3] Mayoral M L *et al* 2014 *Nucl. Fusion* **54** 033002
- [4] Kuriyama M *et al* 1995 *Fusion Eng. Des.* **26** 445
- [5] Zhang M *et al* 2019 *Fusion Eng. Des.* **146** 1712
- [6] Zhang M *et al* 2020 *IEEE Trans. Plasma Sci.* **48** 1688
- [7] Wang J X *et al* 2021 *Plasma Phys. Control. Fusion* **63** 125014
- [8] Yang Y *et al* 2017 *IEEE Trans. Plasma Sci.* **45** 495
- [9] Igiure V M, Laughter S A and Williams R D 2006 *Comput. Secur.* **25** 498
- [10] Xia L L *et al* 2014 *IEEE Trans. Plasma Sci.* **42** 1026
- [11] Watanabe K *et al* 2006 *Nucl. Fusion* **46** S332
- [12] Pesce A, De Lorenzi A and Boldrin M 2011 *Fusion Eng. Des.* **86** 847
- [13] Wang D Y *et al* 2020 *IEEE Trans. Plasma Sci.* **48** 1676
- [14] Xie F, Li G and Cheng D S 2013 *IEEE Trans. Dielectr. Electr. Insul.* **20** 1056
- [15] Roccella R 2019 *Static and Transient Magnetic Field Maps at Level B1 Tokamak Complex Cadarache (France: ITER)*
- [16] Yang Y *et al* 2018 *IEEE Trans. Ind. Electron.* **65** 8204
- [17] Zhu B L *et al* 2022 *IET Electric Power Appl.* **16** 710
- [18] Lu Y W *et al* 2021 *Fusion Eng. Des.* **166** 112302
- [19] Wang R M *et al* 2022 *IEEE Trans. Plasma Sci.* (<https://doi.org/10.1109/TPS.2022.3169476>)
- [20] Wang R M *et al* 2022 *Plasma Sci. Technol.* **24** 124019
- [21] Wang R M *et al* 2021 *Fusion Eng. Des.* **167** 112344
- [22] Rao B *et al* 2022 *Fusion Eng. Des.* **184** 113297
- [23] Liu Z M *et al* 2014 *J. Fusion Energy* **33** 398
- [24] Patel P *et al* 2013 *IEEE Trans. Plasma Sci.* **41** 263
- [25] Mao X H *et al* 2014 *IEEE Trans. Plasma Sci.* **42** 1425
- [26] Ma S X *et al* 2014 *IEEE Trans. Plasma Sci.* **42** 656
- [27] Ma S X *et al* 2015 *J. Fusion Energy* **34** 261
- [28] Ma S X *et al* 2014 *IEEE Trans. Plasma Sci.* **42** 1709
- [29] Xu W D *et al* 2012 *Plasma Sci. Technol.* **14** 263
- [30] Ma S X *et al* 2014 *J. Fusion Energy* **33** 693
- [31] Jin Y K *et al* 2019 *Fusion Eng. Des.* **146** 2654
- [32] Ma S X *et al* 2019 *IEEE Trans. Plasma Sci.* **47** 2937
- [33] Ma S X *et al* 2021 *Fusion Eng. Des.* **169** 112491
- [34] Wang D Y *et al* 2020 *Plasma Sci. Technol.* **22** 085601
- [35] Zhang M *et al* 2015 *J. Fusion Energy* **34** 361

- [36] Zhang X L et al 2019 *Fusion Eng. Des.* **146** 2592
- [37] Wang D Y et al 2021 *Fusion Eng. Des.* **165** 112253
- [38] ABB medium voltage AC drives (<https://new.abb.com/drives/medium-voltage-ac-drives>)
- [39] TMEIC inverter TMdrive-XL55 (<https://tmeic.com/product/tmdrive-xl55>)
- [40] Zhang X L 2019 Research and design of the acceleration grid power supply of CFETR N-NBI prototype *PhD Thesis* Huazhong University of Science and Technology (Wuhan, China) (in Chinese)
- [41] IGCT 5SHY35L4520 (<https://new.abb.com/products/5SHY35L4520/5shy35l4520>)
- [42] IEGT ST1500GXH24 (<https://toshiba.semicon-storage.com/us/semiconductor/product/igbts-iegts/iegt-ppi/detail.ST1500GXH24.html>)
- [43] Zhang M et al 2016 *IEEE Trans. Plasma Sci.* **44** 1716
- [44] Ratti D et al 2021 *Fusion Eng. Des.* **173** 112907
- [45] Zhang X L et al 2019 *IEEE Trans. Plasma Sci.* **47** 1864
- [46] Wang D Y 2021 Research on key technologies of the acceleration grid power supply-conversion system of CFETR N-NBI *PhD Thesis* Huazhong University of Science and Technology(Wuhan, China) (in Chinese)
- [47] Wang D Y et al 2020 *Fusion Eng. Des.* **161** 111917
- [48] Ma S X et al 2022 *IEEE Trans. Plasma Sci.* **50** 1137
- [49] Xuan W M et al 2008 *Nucl. Fusion Plasma Phys.* **28** 136
- [50] Pesce A, De Lorenzi A and Grando L 2009 *Fusion Eng. Des.* **84** 1499
- [51] Zhang M et al 2019 *Fusion Eng. Des.* **146** 2618
- [52] Cao L, Li G and Wang H T 2011 *Plasma Sci. Technol.* **13** 115
- [53] Steurer M et al 2002 *IEEE Power Eng. Rev.* **22** 62
- [54] Chen X et al 2017 *IEEE Trans. Plasma Sci.* **45** 2328
- [55] Ji S Q et al 2018 *IEEE Trans. Ind. Appl.* **54** 4640
- [56] Millán J et al 2014 *IEEE Trans. Power Electron.* **29** 2155
- [57] Hazra S et al 2016 *IEEE Trans. Power Electron.* **31** 4742
- [58] Beaumont B et al 2005 *Fusion Eng. Des.* **75–79** 1281
- [59] Wang D Y et al 2020 *Fusion Eng. Des.* **153** 111483
- [60] Ma S X et al 2021 *Rev. Sci. Instrum.* **92** 024713
- [61] Jiang cc et al 2016 *Rev. Sci. Instrum.* **87** 123302
- [62] Ma S X et al 2022 *IEEE Trans. Plasma Sci.* **50** 747
- [63] Yang S 2021 Key technologies research on high voltage generation stage of the accelerator power supply for CFETR N-NBI prototype *MSc Thesis* Huazhong University of Science and Technology(Wuhan, China) (in Chinese)
- [64] Benfatto I et al 2005 *Fusion Eng. Des.* **75–79** 235
- [65] Hourtoule J et al 2005 *Fusion Eng. Des.* **75–79** 179
- [66] De Lorenzi A et al 2005 *Fusion Eng. Des.* **75–79** 33
- [67] Rao Y 2016 *Test Method for ITER Equipment for Static D.C. Magnetic Fields, Cadarache* (France: ITER)
- [68] IEC 61000-4 Part 8: power frequency magnetic field immunity test document IEC 61000-4 2009 (<https://webstore.iec.ch/publication/4229>)
- [69] DOD-STD-1399 (NAVY)-Section 070-Part 1: DC magnetic field environment 26 February 1979 (http://everyspec.com/DoD/DoD-STD/DOD-STD-1399_070-1_25598/)
- [70] Lu Y W et al 2022 *IEEE Trans. Ind. Electron.* **69** 6350
- [71] Lu Y W, Yang Y and Wang R M 2022 *Meas. Sci. Technol.* **33** 095902
- [72] Lu Y W et al 2022 *IEEE Trans. Magn.* **58** 8001309
- [73] Wang R M et al 2022 *J. Magn. Magn. Mater.* **550** 169125
- [74] Tuszewski M 1988 *Nucl. Fusion* **28** 008
- [75] Lin M N et al 2017 *Rev. Sci. Instrum.* **88** 083507
- [76] Kim M et al 2010 *Fusion Eng. Des.* **85** 515
- [77] Dalesio L R and Davidsaver M A 2018 EPICS 7 provides major enhancements to the EPICS toolkit *Proc. of the 16th Int. Conf. on Accelerator and Large Experimental Control Systems 22 (Geneva)* (JACoW) (<https://doi.org/10.18429/JACOW-ICALEPCS2017-MOBPL01>)
- [78] Zheng W et al 2019 *Fusion Eng. Des.* **146** 2379
- [79] Zheng W et al 2022 *Fusion Eng. Des.* **180** 113138
- [80] Zheng W et al 2020 *Fusion Eng. Des.* **155** 111450